

EE412 Advanced Nanofabrication

**Three-dimensional current collector for advanced  
microbatteries**

Dingchang Lin, Yayuan Liu, and Jie Zhao

## **Abstract**

Bulk-size lithium ion batteries now dominate the portable electronic market, and exhibit great potential for electrical vehicle and grid-scale energy storage. However, the development of biological/medical devices and self-powered microelectronics calls for batteries with smaller size and higher power density. Here, we fabricated a three-dimensional current collector, finger-like platinum bottom with regular nickel pillar arrays. This unique structure enhances both ion and electron transport kinetics in batteries, which potentially enable batteries with higher power density. Using advanced fabrication techniques, the size of the microbatteries can be effectively reduced.

## Introduction

Lithium ion batteries (LIBs) are widely used for consumer electronics and exhibit great potential for electrical vehicle and grid-scale energy storage.<sup>1</sup> The most common commercial LIBs used in these applications are in the forms of pouch cells, coin cells, and cylindrical cells. These batteries are generally bulk in size. The smallest coin cell (ML421) is still above 5 mm in diameter.<sup>2</sup> The rapid development of electronics and information technology towards the directions of multi-functionality, high integration and high power drives the electronic devices towards miniaturization. The continuous downscaling of microelectronics, especially the rapid growth of MEMS devices and biological/medical devices, has created a large demand for high-performance energy storage devices on the millimeter scale or less.<sup>3</sup> Unfortunately, commercial coin cells are still routinely used in these applications due to the lack of commercial cells of small size.<sup>4</sup> The reduction in size and the improvement in the capability of microelectronics are presently limited by the size, capacity and power of their on-board power supplies.

Microbatteries are the ideal energy storage devices for these microelectronics. Although capacitors can also be integrated into electronics, few capacitors have energy density approaching that of batteries.<sup>5</sup> Batteries can store considerably more energy than capacitors, but deliver lower power than capacitors and have proven difficult to miniaturize and integrate. Power density of energy storage devices are highly influenced by ion/electron transportation distance and the surface area of electrodes.<sup>6</sup> It is well known that reductions in the characteristic dimensions of the electrolytically active material are effective in improving battery power density, because the characteristic time constant  $t$  for diffusion is proportional to the square of the diffusion length  $L$  ( $t \approx L^2/D$ ).<sup>7</sup> The enlarged electrode surface area could increase the allowed current and amount of materials deposited, therefore enhancing the areal energy and power densities.<sup>8</sup> In principle, a microbattery architecture based on 3D integrated microelectrodes could achieve high-power density without sacrificing energy density by combining small ion diffusion distances, high surface area and large percentage of active materials. Such microarchitecture could also enable miniature batteries suitable for microelectronics integration.

Here, we use multiple steps to fabricate a 3D current collector, platinum finger electrode with regular nickel (Ni) pillar arrays ((1) Pattern the platinum finger electrodes on the oxidized Si wafer. (2) Pattern

the template for arrays on the finger electrodes. (3) Using electroplating to deposit nickel pillar arrays.). This unique 3D current collector effectively minimizes the ion diffusion distance and enlarges the surface area of the electrode. Micro-fabricating 3D current collector with high aspect ratios followed by deposition of battery layers potentially enables microbatteries with higher power density.

## Experimentals

To fabricate the 3D current collector as we proposed above, we designed an approach using photolithography, e-beam evaporation and electroplating technologies subsequently. **Figure 1** shows our design and fabrication process for the 3D current collector. As is shown in the figure, first of all, parallel finger electrodes with various distances between two fingers (72  $\mu\text{m}$  to 180  $\mu\text{m}$ ) were designed and patterned. The finger electrode patterns were designed for the deposition of Pt layer as the conductive current collector of the cathode and anode. Once the finger electrodes were fabricated, on the top of the finger electrodes, the dot arrays with diameter of dots varied from 10  $\mu\text{m}$  to 30  $\mu\text{m}$  were designed. The dot arrays will become open space later in photolithography process for the fill in of Ni metal through electroplating. After the Ni plating, the current collectors will become the array of Ni micropillars standing on the Pt finger electrodes on the substrates. This design will expand the electrode to the third dimension and increase the active area of the current collector for active electrode material loading and simultaneously improve the diffusion kinetics.

To fulfill the fabrication of the finger electrodes, the first layer of photolithography was applied. 1.5  $\mu\text{m}$  of SPR3612 positive photoresist was firstly coated onto Si wafer substrates with SVG coater. The Si wafers used as the substrate were thermally oxidized to obtain  $\sim 200$  nm of  $\text{SiO}_2$  layer for insulation, followed by the pre-treatment in HMDS atmosphere (YES oven) for good photoresist adhesion. After the coating of SPR 3612 photoresist, the wafer was exposed under 365 nm ultra-violet (UV) light for 1.5s (Karlsuss, 15  $\text{mW}/\text{cm}^2$ ). The as-exposed wafers were then developed with Shipley MF-26A for 2 minutes with the SVG developer to obtain sharp patterns. Afterward, electron-beam evaporation was performed to deposit Ti (20 nm)/Pt (200 nm) layer onto the substrate, followed by the removal of

photoresist to yield the clean substrates with Pt finger electrodes.

To construct the pillar arrays onto the Pt finger electrodes, the second layer of photoresist was applied as the template. Since micropillars with higher aspect ratio will be favorable, thick photoresist layer is needed here. In this work, SPR 220-7, which is widely used for thick photoresist coating, was used here. Before the photoresist coating, the finger electrode substrates were treated in HMDS atmosphere again for good photoresist adhesion. Then, the photoresist coating was performed with SVG coater at 1000 rpm, which gives ~15  $\mu\text{m}$  with one coat. To obtain thicker photoresist, multiple coats of SPR 220-7 photoresist need to be applied. In this work, up to 3 coats were performed on a single finger electrode substrate to afford the thick photoresist up to ~45  $\mu\text{m}$ . The exposure of the thick photoresist is a challenge, to get better contrast after exposure, the exposure time should be optimized. Multi-exposure is preferred while rest between two exposure will help avoid the formation of bubbles inside the photoresist and get thorough exposure. The detailed parameter of exposure time will be discussed in-depth in the next session. The develop process is also critical. Manual develop was performed here with Shipley MF-26A developer, while the develop time was varied from 5 min to 8 min.

To perform electroplating of Ni micropillars, the devices were first subjected to oxygen plasma treatment for 5 min and subsequently mounted on to a glass substrate. Specifically speaking, the major areas of the Pt side bars were taped to a glass substrate to prevent Ni plating directly onto the side bars. Aluminum wire bonding (25  $\mu\text{m}$  wire) was then performed to connect the exposed Pt side bars to an aluminum tape on the glass substrate, where alligator clips can be used to connect the device to the potentiostat (BioLogic VMP3). The device is was set as the cathode of the electroplating cell while a high-purity Ni foil was set as the anode. The plating was carried out in commercial Ni electroplating solution (KROHN Bright Nickel Electroplating Solution) at room temperature with a constant magnetic stirring of 200 rpm. Constant current electroplating was used where the height of the electroplated Ni micropillars can be controlled by the deposition time.

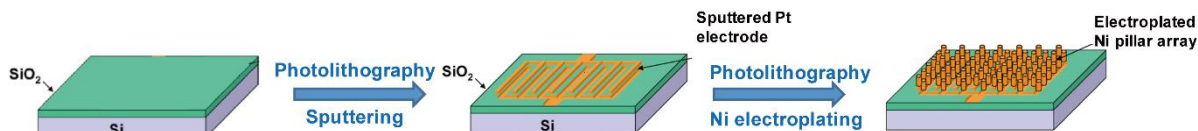


**Figure 1. Schematic.** Schematic figure showing the fabrication procedure of the 3D current collector for microbattery.

## Results and Discussions

### Photomask design

To fulfill our design of the 3D current collector, photomasks with various spacing were designed here. The dark area as shown in **Figure 2a** and **b**, was the open space for exposure under UV light. With the positive photoresist SPR 3612, the exposed area will be developed and leave the trench for Pt deposition. The magnified images of the patterns, as shown in **Figure 2c** and **e**, clearly show the detailed design of microstructures. The finger electrodes, as shown in **Figure 2c**, were connected separately to two metal pads on its two ends. The nearby two lines were connected to different pads which can guarantee the shortest diffusion pathway between the two electrodes. Although the 2D finger electrodes can decrease the diffusion distance, the surface area for active material loading is limited. The design of the third dimension is favorable to further increase the active surface area and reduce the diffusion limit. As a consequence, the micropillar array patterned directly on the finger electrodes were further designed. As shown in the magnified image in **Figure 2d**, after combining the first and the second layer of the pattern, the as-obtained pattern has the dot array right on the top of finger electrodes. The 3D schematic drawing in **Figure 2f** more clearly shows the design of the 3D current collectors.

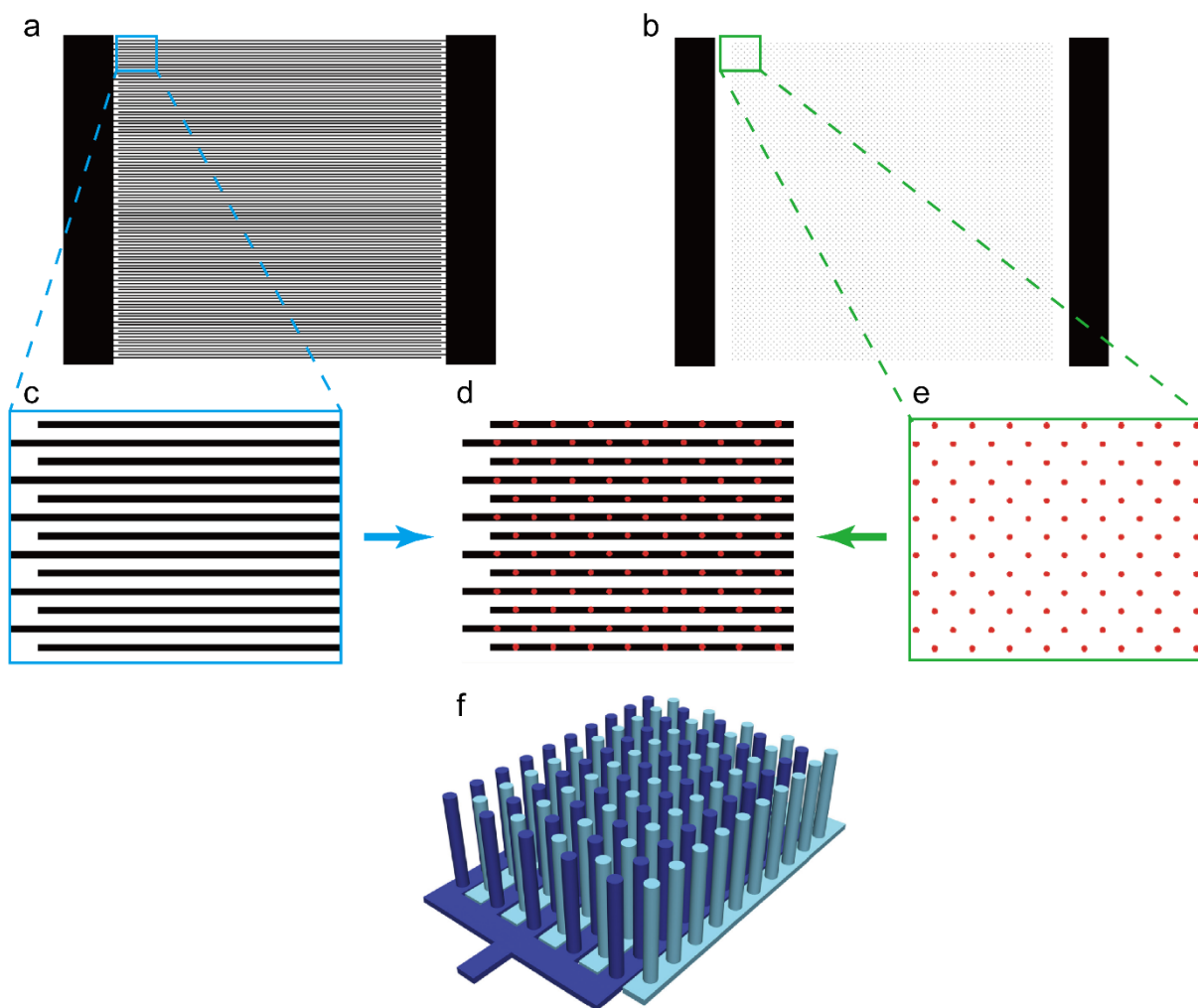


**Figure 2. Pattern design of the photo mask.** **a**, Design of finger electrode pattern for the first layer. The corresponding magnified image of the finger electrodes is shown in **c**. **b**, Design of the dot arrays pattern for the second layer. The corresponding magnified image of the dot arrays is shown in **e**. **d**, the combined pattern of the first and second layer of photolithography, where the dot arrays are patterned on the finger electrodes.

To further study the effect of the finger electrode spacing on their electrochemical performance, different spacing of the finger electrodes was designed here. As shown in **Figure 3**, A represents the spacing between two nearby electrodes lines connected to the same electrode pad, while B represent the width of the electrode lines which is the same as the diameter of the dots. In this work, we varied A from 10  $\mu\text{m}$  to 30  $\mu\text{m}$ , while B was tuned from 72  $\mu\text{m}$  to 180  $\mu\text{m}$ . The resulting finger patterns we obtained were shown in **Figure 4**. **Figure 4a** shows the wafer after Ti (20 nm)/Pt (200 nm) thin film deposition, while **Figure 4b** shows the wafer after residual photoresist removal. The wafer after photoresist removal

exhibited clean surface with minimal photoresist residue. **Figure 4c** shows the optical microscope image of the finger electrodes with the width of  $\sim 10$   $\mu\text{m}$ . Although slightly rough edges can be observed due to the limited resolution of transparency photomask, the electrode strips showed relatively shape edge, which is good enough for our purpose.

Different spacing of the finger electrodes are further shown in **Figure 4d-h**, which are A10-B72, A10-B100, A15-B120, A20-B120, and A30-B180, respectively. All the finger electrodes show shape edges without break of fingers or shorting, which paves the way for later electroplating process and the fabrication of 3D current collectors.

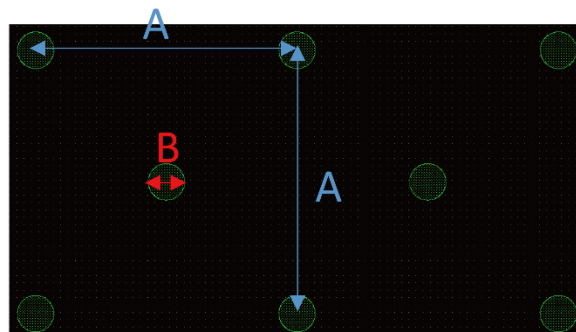


**Figure 3. Dimension of the design.** Dimension of the finger electrode and dot arrays design. A is the distance between two neighbor rows of the same electrode. B is the diameter of the dot, which is the same as the width of the finger electrode.



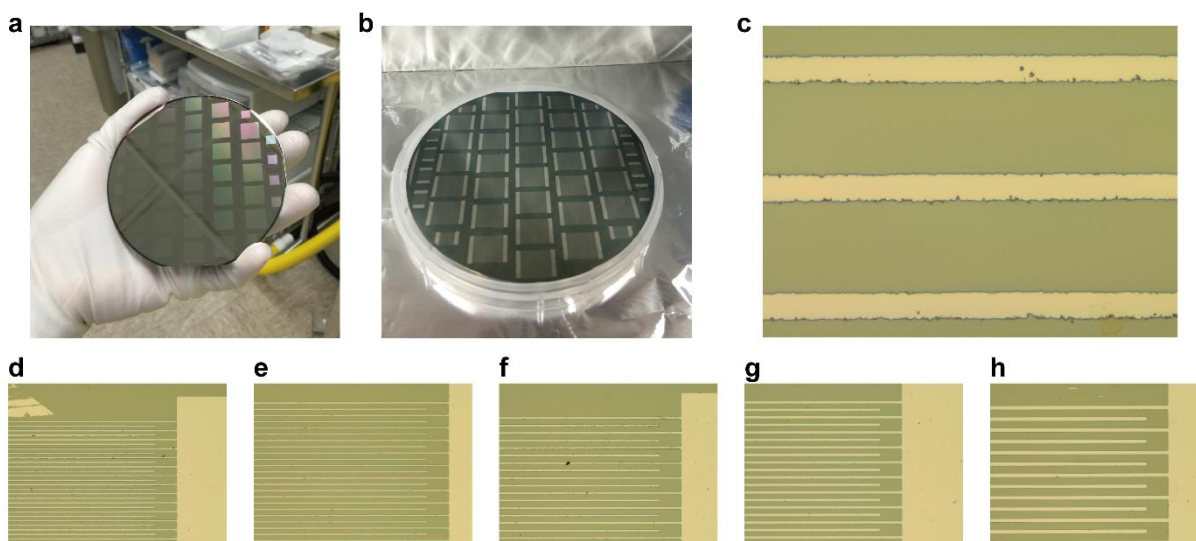


**Figure 4. Fabrication of the finger electrodes.** **a**, Photo image of the wafer with patterned structure after Pt deposition. **b**, Photo image of the wafer after the removal of the photoresist, which yields the pattern of the finger electrodes on the wafer. **c**, The optical microscope image of the smallest feature of the finger electrode we design (width = 10  $\mu\text{m}$ ). **d-h**, the optical microscope image of the finger electrodes with different dimension of the fingers varied from 10  $\mu\text{m}$  to 30  $\mu\text{m}$ . **f**, Schematic 3D image showing the as-designed 3D current collector. The dark and light blue colors are corresponding to two separator electrodes.

### Thick photoresist

After the fabrication of Pt finger electrodes, Ni micropillars need to be patterned on the top. In this work, photoresist mold with patterned open dots was used as the template for Ni micropillar growth. Since the diameter of the Ni micropillars was in the range of 10-30  $\mu\text{m}$ , it is necessary to fabricate the pillars with height of 30-45  $\mu\text{m}$  to obtain high enough aspect ratio. As a consequence, thick photoresist of 30-45  $\mu\text{m}$  needed to be employed in this work.

For conventional 2D patterning, only thin layer of photoresist with  $\sim 1-3$   $\mu\text{m}$  thickness is required. The photoresist we need here is actually 20-40 times thicker than most of the situations. The dramatic increase in thickness will bring about several challenges: (i) High resolution and sharp edge is harder to be obtained. (ii) The level of exposure at different depth will be various drastically. (iii) Long-time exposure is needed, which might generate bubbles in the exposed area and affect the further exposure.

In this work, SPR 220-7 was used as the photoresist. One layer of SPR220-7 spin coated at 1000 rpm

gives ~15 um. As a consequence, 2-3 coats were needed in our work.

For multiple coats of photoresist, post-bake is crucial to afford dry and uniform photoresist. We first tried post-baking the photoresist after multiple coating in the box furnace at 90 °C. However, bubbles were trapped inside the photoresist after baking. This process was then modified to be 200s post-bake at 90 °C hotplate after each coat. The as-obtained photoresist molds were kept in the yellow room for 1 day to afford fully dried photoresist as shown in **Figure 5a**.

The exposure time is another critical parameter. Single exposure with various exposure time from 60 s to 200 s was first applied on 2 coats of photoresist. However, the exposure time was still not enough to afford thorough pores. Even though 200 s was too short, bubbles started to be generated in the exposed area and forbidden further uniform exposure. As a consequence, multi-exposure is introduced here.

For multi-exposure, 15 s exposure followed by 15 s rest was applied as one cycle. For 2 coats of photoresist, we found that 20 cycles of exposure, with 300 s of exposure time in total is enough to obtain shape feature. For 3 coats of photoresist, 34 cycles of exposure is appropriate for full exposure.

After exposure, manual develop with Shipley MF-26A was performed. 5 min develop was applied for 2 coats while 8 min was employed for 3 coats.

**Figure 5b-e** shows the optical microscope images of the photoresist mold after develop. **Figure 5b, c** shows the photoresist with 30 um pores, while **Figure 5e,f** shows the photoresist with 20 um pores. Both the samples exhibited fully open features after develop with relatively sharp edge. However, for the 10 um feature, as shown in **Figure 5d**, no thorough pores can be obtained. This can be due to the resolution limit of the transparency photomask on thick photoresist, where small surface roughness of photoresist will affect the contact between mask and substrate and reduce the resolution.

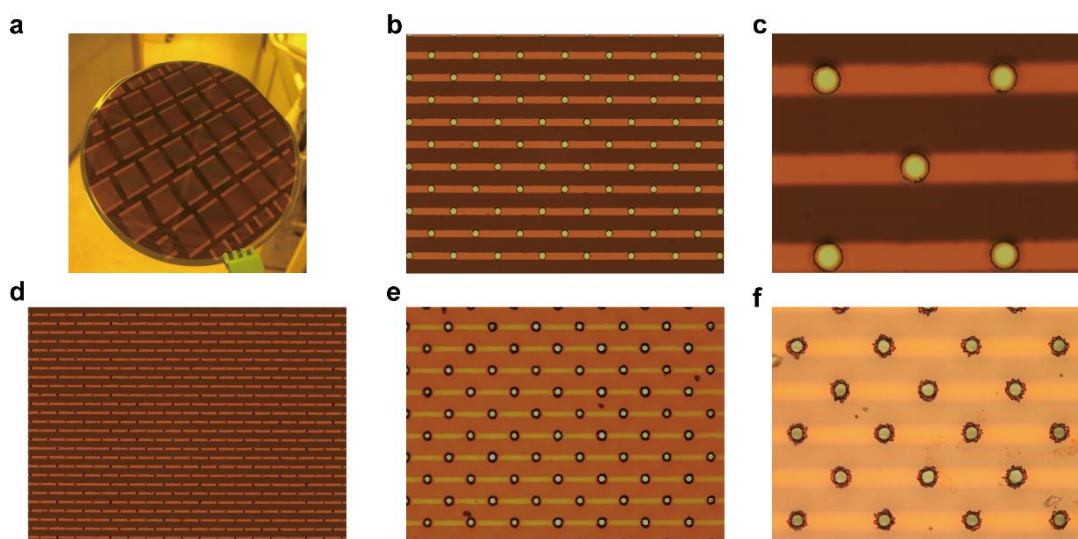


**Figure 5. Photos resist pattern of the second layer of dot arrays.** **a**, Digital camera image of the second layer photoresist ( $\sim 30$   $\mu\text{m}$ ) on the finger electrode substrate. **b**, Optical microscope image of the patterned second layer on the substrate with 30  $\mu\text{m}$  in diameter of the dots. **c**, Magnified image of the patterned dot arrays shown in **b**. **d**, Optical microscope image of the patterned second layer on the substrate with 10  $\mu\text{m}$  in diameter of the dots. **e**, Optical microscope image of the patterned second layer on the substrate with 15  $\mu\text{m}$  in diameter of the dots. **f**, Magnified image of the patterned dot arrays shown in **d**.

### Ni electroplating

The experimental setup employed for Ni electroplating was shown in **Figure 6**, where the device chip was mounted on a glass substrate with the two side Pt bars covered to prevent direct deposition (**Figure 6a**). The device was connected to an aluminum tape on the glass substrate via wire bonding, which could subsequently be connected to potentiostat using alligator clips (**Figure 6b** is a digital photo image of the device). As can be seen from **Figure 6c**, two-electrode plating setup was used with our device as the cathode/reference electrode and a high-purity Ni foil as the anode. The plating solution was immersed in 50  $^{\circ}\text{C}$  water bath with constant magnetic stirring to aid ion diffusion, and thus, a more homogenous deposition. Noticeably, a constant current deposition was used to precisely control the amount of charges passed through, which in turn determines the height of the electrodeposited Ni micropillars.

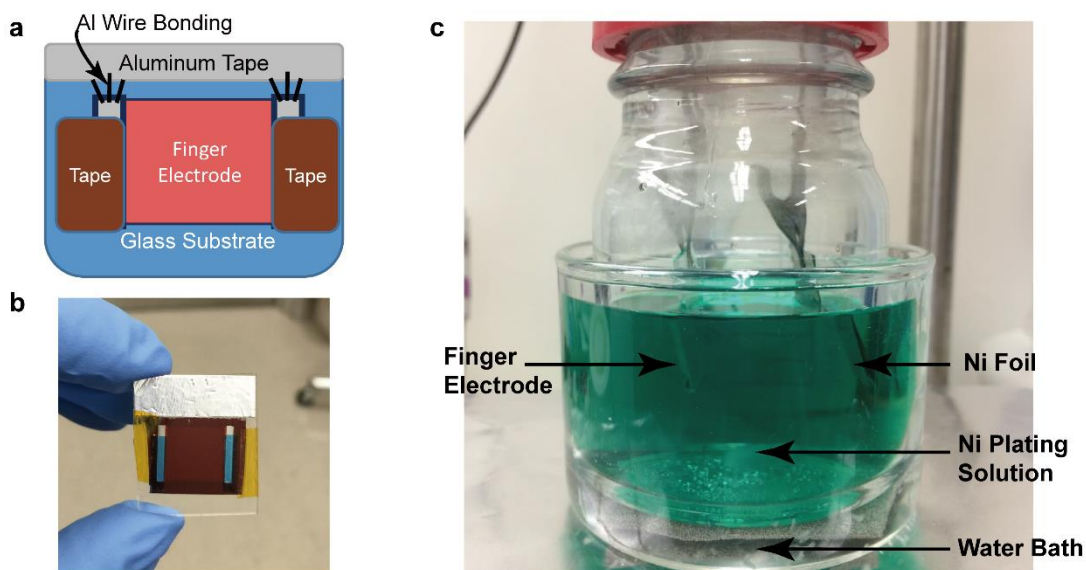


**Figure 6. Ni electroplating setup.** **a**, Schematic figure showing the design of the finger electrode connection for Ni plating. **b**, Digital camera image of the device as described in **a**. **c**, Digital camera image of the setup for Ni plating, where the cathode and anode were immersed into the Ni plating bath and an external power source was used to supply the current for Ni deposition.

To clearly see the effect, side-sided plating was performed first where only one side of the finger electrode was connected to the external circuit (**Figure 7a**). It was found that the wetting of the Ni plating solution into the micropores of the photoresist mold was poor, as a result, the plating voltage was extremely high even at a relatively low plating current density ( $0.3 \text{ mA/cm}^2$ ). The high plating voltage started splitting water, generating an excessive amount of bubbles that damaged the photoresist mold quickly (**Figure 7b**). Nevertheless, by a simple oxygen plasma treatment (5 min) prior to electroplating, the wetting of the photoresist mold was improved significantly, leading to the successful reduction in electroplating potential ( $\sim 1\text{V}$ ). **Figure 7c** shows the optical microscopy image of the electrode after depositing  $0.1 \text{ mAh/cm}^2$  of Ni, where the pores connected to the external circuit were filled with a layer of Ni judging from the color contrast. The scanning electron microscope (SEM) image of the electrode at the corresponding deposition state is shown in **Figure 8c**, where only a thin layer of Ni ( $\sim 2 \text{ }\mu\text{m}$  in thickness) can be seen.

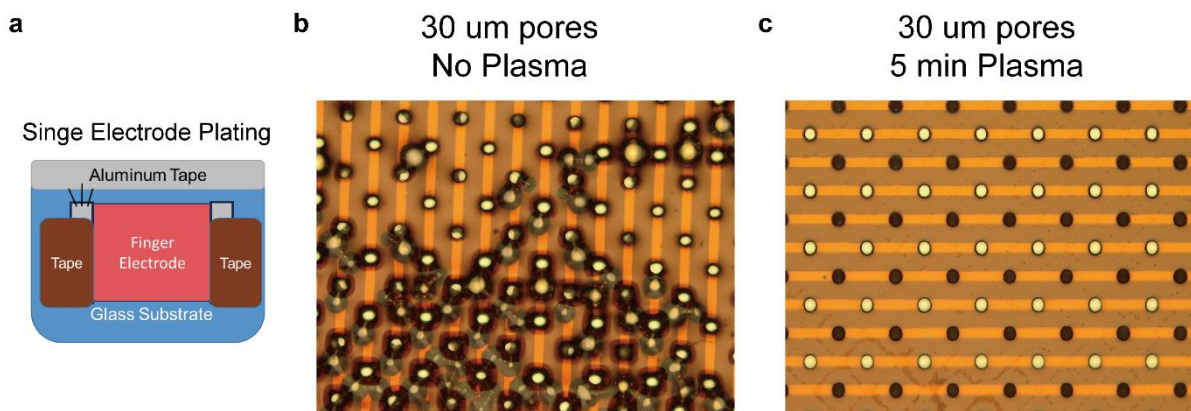


**Figure 7. Electroplating with single-side connection.** **a**, Schematic figure showing the design of the single-side connection for electroplating. **b**, Optical microscope image of the deposition without plasma treatment on the photoresist **c**, Optical microscope image of the deposition with 5 minute plasma pretreatment on the photoresist.

In order to increase the aspect ratio of the electroplated Ni micropillars, more Ni needed to be deposited. However, when the deposition amount was increased from  $0.1 \text{ mAh/cm}^2$  to  $1.5 \text{ mAh/cm}^2$ , instead of forming straight micropillars, mushroom-shaped Ni deposition morphology was observed (**Figure 8b, d**). We suspected that the uneven deposition behavior shall be attributed to the limitation of our homemade Ni plating solution (Watts solution). Namely, without special additives in the plating electrolyte, it can be challenging to obtain uniform deposition with small grain size and smooth surface. According to literature,<sup>9</sup> deposits from Watts solutions without additives are soft and often with varying degrees of evenness. However, the appearance and properties can be dramatically changed by the use of addition agents, for the addition agents consist of organic and certain metallic compounds selected to brighten and level the deposits. For example, anionic surfactants anti-pitting agents/wetting agents, such as sodium lauryl sulphate are usually included in commercial Ni plating solutions to lower the surface tension of the solution and to facilitate release of hydrogen bubbles in order to obtain a more even deposition. As a result, we also tested out a common commercial Ni plating solution (KROHN Bright Nickel Electroplating Solution), which indeed gave rise to much improved deposition stability in terms of voltage (remained constant for more than 7 hrs for two-coats photoresist mold) and deposition morphology.

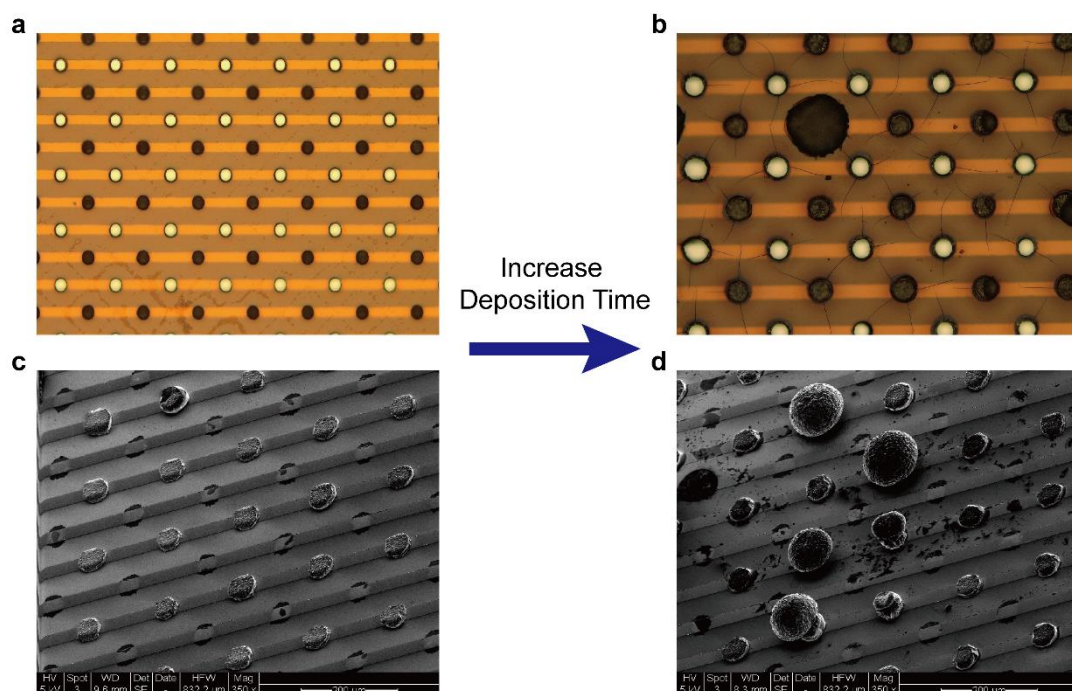


**Figure 8. Electroplating with different plating time.** **a, c**, Optical microscope and 45 ° scanning electron microscope images of the Ni plating into the 30 μm pores at current density of 0.3 mA and deposition capacity of 1.5 mAh. **b, d**, Optical microscope and 45 ° scanning electron microscope images of the Ni plating into the 30 μm pores at current density of 0.3 mA and deposition capacity of 3 mAh.

**Figure 9** shows the SEM images of the electroplated Ni micropillars using the commercial Ni plating solution and 2-coats (30 μm) photoresist mold. 5.5 mAh/cm<sup>2</sup> of Ni was plated, which is the amount that can fill the photoresist pores without protruding out. As can be seen from **Figure 9a and b**, Ni disks can be obtained by electrodepositing into 30 μm pore photoresist mold, which has a theoretical aspect ratio of 1:1. And if photoresist mold with 15 μm pore was used (theoretical aspect ratio of 2:1), distinctive micropillar features can be observed clearly (**Figure 9c and d**). Importantly, smooth pillar side walls can be seen from the magnified SEM images, confirming the merits of the commercial Ni plating solution.

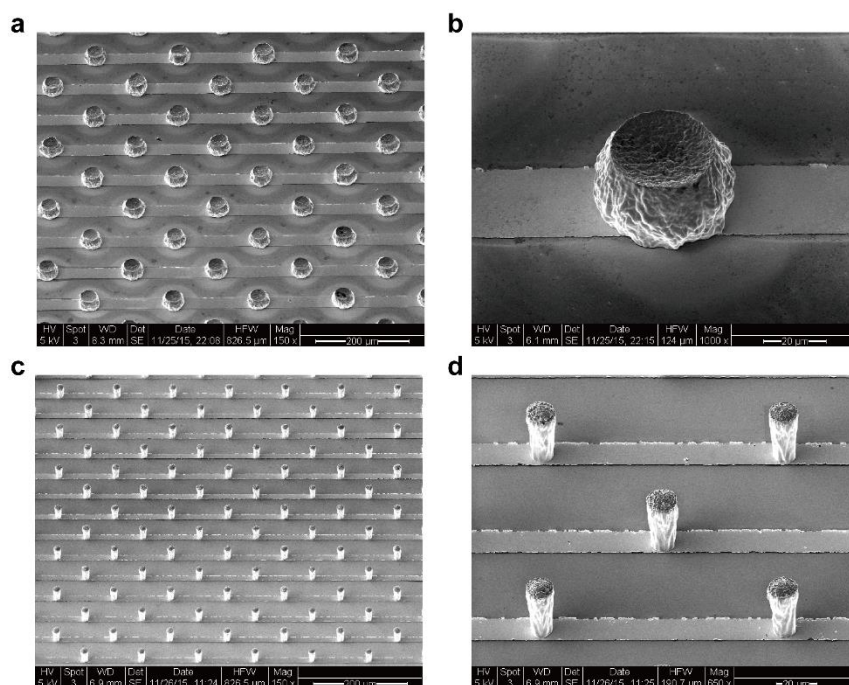


**Figure 9. Pillar array on finger electrodes with ~30 μm photoresist. a,** SEM image of the micropillar array with the pillars' diameter of ~30 μm. **b,** Magnified SEM image of a single 30 μm micropillar showing the typical morphology of the pillar. **c,** SEM image of the micropillar array with the pillars' diameter of ~15 μm. **d,** Magnified SEM image of a single 15 μm micropillar showing the typical morphology of the pillar.

Finally, in order to obtain Ni micropillars with even higher aspect ratio, which is desirable for high-surface area 3D battery current collectors, Ni electroplating using 3-coats (45 μm) photoresist mold was also attempted. The amount of Ni plated was increased proportionally according to the photoresist thickness (5.5 mAh/cm<sup>2</sup> for 2-coats, thus, 8.5 mAh/cm<sup>2</sup> for 3-coats). However, as can be seen from **Figure 10**, the aspect ratio of the micropillars did not increase significantly as expected. We found out that as we prolong the electroplating time, the tape that was used to cover the two Pt side bars can deteriorate and detach. This will result in excessive Ni plating directly on the side bars, due to the reduced Ni ions diffusional barrier. As a result, the height of the Ni micropillars did not increase significantly in the case of 3-coats photoresist mold.

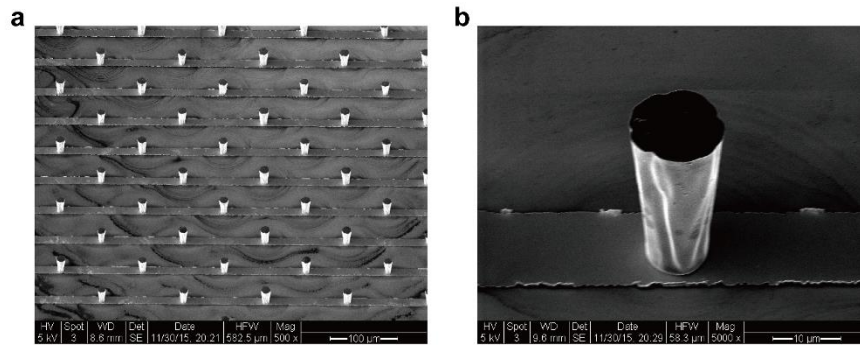


**Figure 10. Pillar array on finger electrodes with ~45 µm photoresist.** **a**, SEM image of the micropillar array with the pillars' diameter of ~15 µm. **b**, Magnified SEM image of a single 15 µm micropillar showing the typical morphology of the pillar.

The experience mentioned above can actually help us to design the electroplating device better in the future. Instead of exposing the side bars, we can actually cover the major areas with photoresist during and only expose a small portion for wire bonding during the electroplating step, as illustrated schematically in **Figure 11**. This improved cell design can effectively prevent depositing on the side bars and the possible shorting caused, affording a more uniform and controllable Ni micropillar morphology.

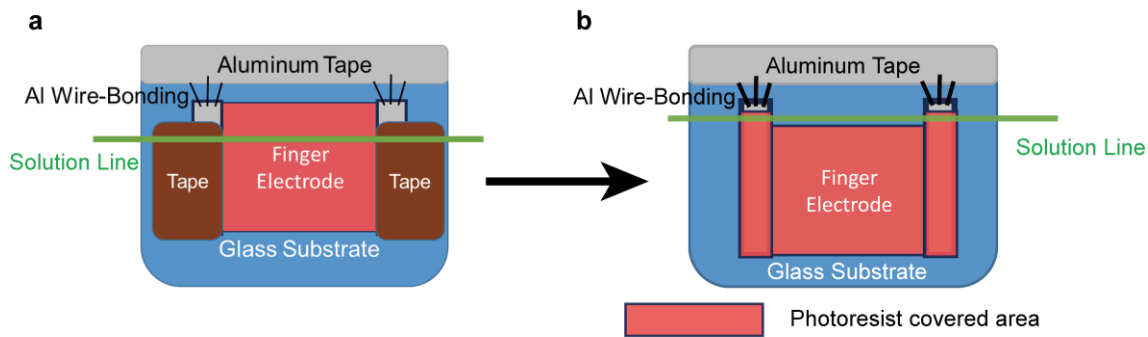


**Figure 11. Modified design for second layer photoresist pattern.** **a**, the original design of the second layer photoresist pattern, which require tapes to cover the electrode pads. **b**, the modified design of the second layer photoresist pattern, which use photoresist to cover the electrode pads.



## Conclusions and Future Work

In conclusion, in this study, we successfully fabricated a 3D microbattery current collector on Pt finger electrode via Ni electroplating with an aspect ratio of at least 2 to 1. In order to obtain a photoresist mold for Ni plating, SPR 220-7 photoresist was employed. Various resist coating, exposure and development parameters were tried out to obtain electroplating molds up to 45  $\mu\text{m}$  thick with feature size down to 15  $\mu\text{m}$ . Different Ni electroplating parameters were tested under the constant current plating regime, where it was found that the commercial Ni plating solution can afford more uniform electroplating morphology. In the future, better device design is required to further increase the aspect ratio of the electroplated Ni micropillars. Electrochemically active materials shall also be electroplated on the 3D Ni current collector to make a full cell battery.

## References

- 1 Goodenough, J. B. & Manthiram, A. A perspective on electrical energy storage. *Mrs Communications* **4**, 135-142, doi:10.1557/mrc.2014.36 (2014).
- 2 Wang, Y. X. *et al.* Lithium and lithium ion batteries for applications in microelectronic devices: A review. *Journal of Power Sources* **286**, 330-345, doi:10.1016/j.jpowsour.2015.03.164 (2015).
- 3 Pikul, J. H., Zhang, H. G., Cho, J., Braun, P. V. & King, W. P. High-power lithium ion microbatteries from interdigitated three-dimensional bicontinuous nanoporous electrodes. *Nature Communications* **4**, doi:Artn 1732 10.1038/Ncomms2747 (2013).
- 4 Tarascon, J. M. & Armand, M. Issues and challenges facing rechargeable lithium batteries. *Nature* **414**, 359-367, doi:Doi 10.1038/35104644 (2001).
- 5 Arico, A. S., Bruce, P., Scrosati, B., Tarascon, J. M. & Van Schalkwijk, W. Nanostructured materials for advanced energy conversion and storage devices. *Nature Materials* **4**, 366-377, doi:10.1038/nmat1368 (2005).
- 6 Kang, B. & Ceder, G. Battery materials for ultrafast charging and discharging. *Nature* **458**, 190-193, doi:10.1038/nature07853 (2009).
- 7 Bruce, P. G., Scrosati, B. & Tarascon, J. M. Nanomaterials for rechargeable lithium batteries. *Angewandte Chemie-International Edition* **47**, 2930-2946, doi:10.1002/anie.200702505 (2008).
- 8 Zhang, H. G., Yu, X. D. & Braun, P. V. Three-dimensional bicontinuous ultrafast-charge and -discharge bulk battery electrodes. *Nature Nanotechnology* **6**, 277-281, doi:10.1038/Nnano.2011.38 (2011).
- 9 Santos, A., Vojkuvka, L., Pallares, J., Ferre-Borrull, J. & Marsal, L. F. Cobalt and Nickel Nanopillars on Aluminium Substrates by Direct Current Electrodeposition Process. *Nanoscale Res Lett* **4**, 1021-1028, doi:10.1007/s11671-009-9351-5 (2009).